ESTIMATION OF TOTAL SURFACE AND SUBSURFACE MELTWATER AMOUNTS ACROSS GREENLAND ICE SHEET

Alamgir Hossan¹, Andreas Colliander¹, Julie Miller², Shawn Marshall³, Joel Harper⁴, Baptiste Vandecrux⁵

¹Jet Propulsion Laboratory, California Institute of Technology, ²Cooperative Institute for Research in Environmental Sciences, University of Colorado Boulder, ³Department of Geography, University of Calgary, ⁴Department of Geosciences, University of Montana, ⁵Geological Survey of Denmark and Greenland

ABSTRACT

Greenland ice sheet (GrIS) melting has been a significant concern in the warming climate. Accurate quantification of total surface and subsurface meltwater amount across the pan-Greenland scale is crucial to understanding GrIS mass balance, thus better projecting global sea level rise. We used multi-year L-band observations from the NASA Soil Moisture Active Passive (SMAP) mission to quantify the GrIS surface and sub-surface meltwater amount and examine their spatiotemporal variability. We employed an empirical algorithm to detect surface and subsurface melt events. Then, we applied a physics-based retrieval algorithm to estimate the intensity and physical properties of the melt events. Finally, we validated the retrieval by meltwater derived from a locally calibrated energy balance model with in situ observations from the PROMICE automatic weather station (AWS) network. The retrieval and validation results are presented, which demonstrate generally a good agreement with the meltwater amounts derived from in situ observations.

Index Terms— Greenland ice sheet, meltwater, SMAP, L-band radiometry, sea level rise

1. INTRODUCTION

The Greenland ice sheet continues to experience an accelerated melting in the last few decades due to climate warming [1], [2]. The meltwater runoff is one of the major contributors to the global sea level rise [3]; nevertheless, a almost 50% of the meltwater percolates through the porous space of the firn – the transitional snow that survives at least a melt season – and is retained there, potentially buffering additional sea level rise [4]. However, with intense and frequent melt events, thick ice layers, called ice slabs, are formed from meltwater refreezing, which prevents vertical percolation of meltwater but increases horizontal runoff [3], [5]. This adverse effect gradually diminishes the ice sheet's inherent capability to retain meltwater and buffer sea level rise [4]. To understand ice sheet dynamics and project sea

level rise accurately, quantifying total surface and subsurface meltwater is essential.

Ice sheet models parametrize melt processes in various ways, resulting in large uncertainties in estimating meltwater [6]. The in situ AWS networks provide much of the desired information where available [7], but whole ice sheet-wise coverage is infeasible with them. Satellite-based observations, especially microwave radiometers, provide an effective and reliable way of monitoring ice sheet melting across the pan-Greenland scale because of their sensitivity to meltwater and global coverage in all weather conditions [8]. However, conventional approaches employing highfrequency bands (i.e., 18 or/and 36 GHz) from heritage radiometers [9], [10] can only track the surface and nearsurface binary melt status, not the meltwater propagation into the deeper layers because of their limited penetration [8]. While the emergence of L-band (1 - 2 GHz) radiometry, marked by the launch of ESA's Soil Moisture and Ocean Salinity (SMOS) mission (November 2009 - present) and the collaborative effort between NASA and Argentina's space agency CONAE in the Aquarius mission (October 2011 -June 2015), followed by NASA's Soil Moisture Active Passive (SMAP) mission (March 2015 - present), has opened up possibilities for monitoring ice sheet meltwater at greater depths, only a few attempts have been made to quantify the overall intensity of meltwater [11], [12]. In this paper, we use multi-year L-band observations from SMAP to quantify the total amounts of surface and subsurface meltwater on the Greenland ice sheet and examine their spatial and temporal variability. L-band signals can penetrate deeper and provide a more accurate estimate of sub-surface meltwater [8], [11], [12].

2. METHODS

We used SMAP L-band enhanced-resolution (3.125km) high-quality Calibrated Passive Microwave Daily Equal-Area Scalable Earth (EASE) Grid 2.0 Brightness Temperature (CETB) gridded (Level 3) data products generated using the radiometer form of the Scatterometer Image Reconstruction (rSIR) algorithm and provided by the

National Snow and Ice Data Center (NSIDC) [13]. The rSIR algorithm leverages the measurement response function (MRF) of each observation and combines the overlapping MRFs to reconstruct enhanced-resolution TB images. The effective resolution of the SMAP rSIR TB products posted on a 3.125 km grid is ~30 km compared to the ~40 km effective resolution of SMAP original data products [13]. CETB provides two TB images daily – corresponding to the local overpass time of the ascending and descending parts of the orbit, facilitating the resolution of diurnal variability. The spatial resolution enhancement enables a more detailed characterization of the heterogeneity of the melt-initiated ice sheet processes.

First, a physics-based empirical algorithm detects surface and subsurface melt events. Because of a large contrast between the dielectric properties of pure ice and pure water ($\varepsilon_i \sim 3.2 \text{ vs } \varepsilon_w \sim 81$), the microwave signature is very sensitive to the volume fraction of meltwater present in the snow/firn. Consequently, even a small amount of meltwater results in large variations in the microwave TB response. This allows an effective melt detection and quantification. SMAP radiometer measures both H- and V-polarized TB and is sensitive to meltwater in the snow/firn/ice. However, due to the Brewster angle proximity of SMAP incidence angle (40°), the changes in V-pol emissivity (and thus TBV) are mostly governed by melt-induced changes in snow/firn/ice dielectric constant compared to the H-pol emissivity, which more likely to be affected by snow/firn/ice vertical structures. Therefore, we considered only V-polarized TB for melt detection and retrieval.

TBV was compared to the combined empirical threshold computed during frozen seasons in the spring (first week of April) and fall (last week of October) every year. During spring, TBV is usually highest across the ablation zone (where mass balance is negative), lowest across the percolation zone, and in between in the upper accumulation zone (positive mass balance regions). During melt seasons, TBV decreases in the ablation zone and increases in the percolation and upper accumulation zones. TBV fall response is the same as during the spring season, except that the overall mean TBV level falls to some extent due to increased volume scattering from grain size, density, and other physical changes in the snow/firn properties onset of melt. Therefore, we determine two constant references for pre- and post-melt seasons and a linearly changing transitional reference during the melt season. Then, the combined thresholds were determined empirically based on the variances of TBV during spring and fall seasons, also using *in situ* references on melt conditions.

A geophysical retrieval algorithm was used to estimate the intensity and physical properties of the melt events. The retrieval algorithm consists of a multi-layer forward model [12] that simulates the L-band TBs and an inversion algorithm that minimizes a cost function between the simulated and observed TBs. TB look up tables (LUTs) were generated using forward model by tuning required

physical parameters (physical temperature, density, dielectric constant, dry and wet layer thicknesses etc.) over reasonable ranges obtained by analyzing in situ measurements across GrIS. In the first step of inversion, the frozen season snow/firn density, physical temperature, and dielectric constant are estimated, and using that information, the volume fraction of meltwater (m_v) , and corresponding melt layer thickness (d_{wet}) are determined during the melt season. The total meltwater amount is thus the product of the two, i.e., MWA = $m_v * d_{wet}$ [m].

Finally, the retrieval was validated by comparing with the meltwater amount obtained from an ice sheet surface energy and mass balance (SEMB) model [14] forced by the hourly *in situ* measurements from the PROMICE (the Programme for Monitoring the Greenland Ice Sheet [7]) automatic weather station (AWS) network. The SEMB model was initialized with ice core density profiles and constrained by the sub-surface temperature profiles from respective AWS [2].

3. RESULTS

Figure 1 below compares the SMAP-retrieved meltwater with the meltwater amount derived from the energy balance model forced by in situ measurements at six different PROMICE AWS using 2023 data. The locations and elevations of the AWS are shown in the color-coded map from the MEaSUREs Greenland Ice Mapping Project (GIMP) Digital Elevation Model in the middle. SMAP (the magenta line) has two daily samples unless the data is missing, while in situ AWS (the black line) has hourly samples. Both present the nearinstantaneous amount of the vertically integrated total meltwater amounts in the porous space of the underlying snow/firn/ice layers. The in situ meltwater amounts were derived from pointwise measurements at the AWS locations, whereas SMAP retrievals were estimated from spatially averaged TB over the effective resolution of the satellite footprint. Nevertheless, both curves show a strong agreement in the magnitude and phase of melting and refreezing at all the locations presented. This perhaps indicates that the spatial heterogeneity of melt processes is not acute in these areas.

Fig. 2 shows the multiyear time series of the retrieved meltwater amount at the first three AWSs presented in Fig. 1. At CP1, 2023 marks the most intensive melts since the launch of SMAP in 2015. MWA in 2015, 2019, and 2021 at CP1 has also been significant. At DY2, the highest melting was observed in 2016 and 2023, but MWA in the other years in SMAP lifetime, except in 2017 and 2022, were significant. There was a six-week gap in SMAP data acquisition from Aug - Sept in 2022. On the other hand, KAN_U has experienced almost constant melt every year except in 2017 and 2020, when the MWA was moderate.

Finally, Fig. 3 depicts the sum of the total daily (evening passes) MWA for every year for 2015 - 2023. The meltwater that existed more than one evening was counted multiple times. So, this is not the total yearly melt, but a

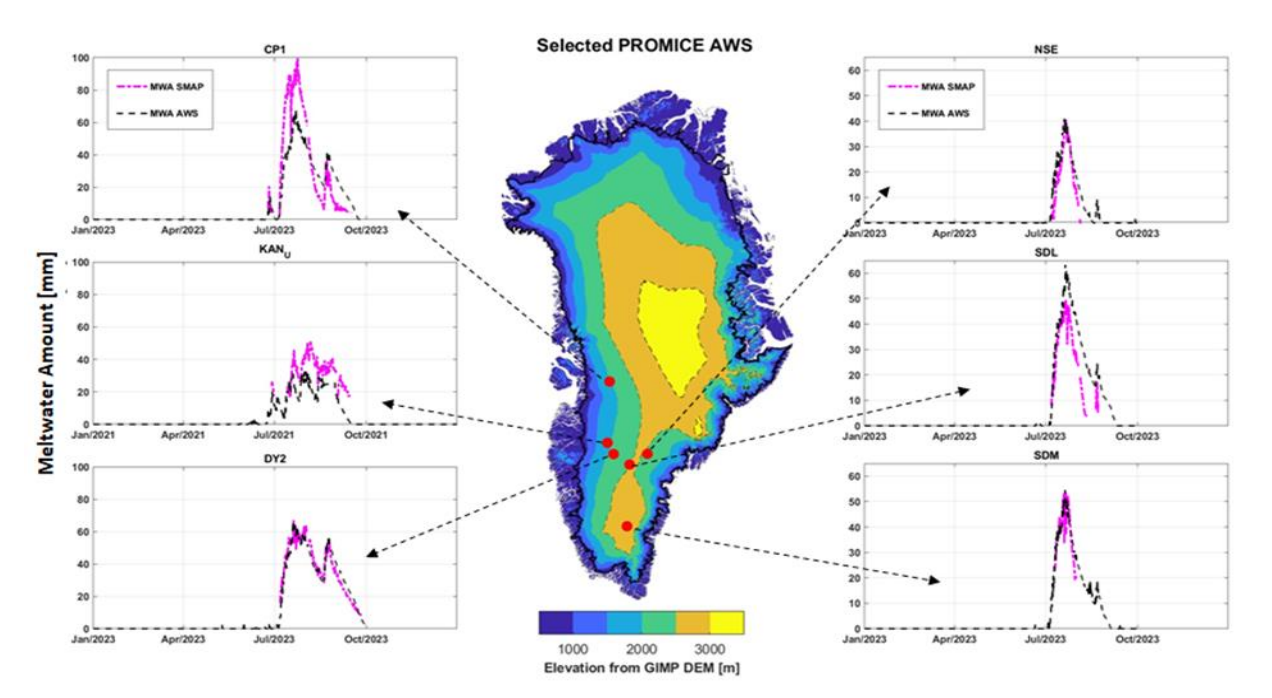


Fig. 1: Comparison of SMAP retrieved total meltwater amounts with selected PROMICE AWS within the GrIS percolation area.

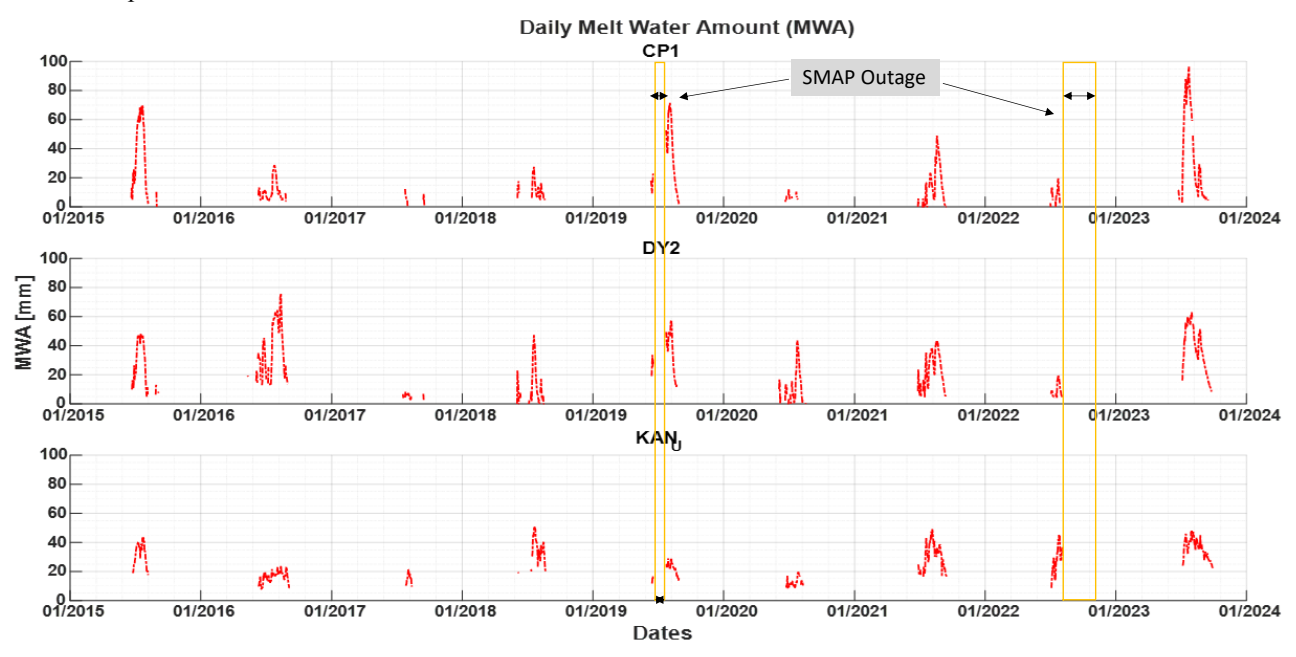


Fig. 2: Time series of SMAP retrieved total meltwater amounts during 2015-2023 period at three PROMICE AWS located at the south-western side of the GrIS.

measure of the total meltwater amount over these areas. In addition, in this work-in-progress maps, we masked out the ablation and higher accumulation areas where melt was detected by a decreasing TB. SMAP can detect the melt events in these areas. However, the hydrological features of the bear ice ablation zone are significantly different from the percolation or upper accumulation zone. This horizontal runoff region is characterized by widespread networks of

supraglacial lakes and rivers, crevasses, and other complex heterogenous factors, such as surface topography, dust deposition, slush saturation etc. This generates an intricate radiometric response, which might require an integrated approach combining the other bands and high-resolution observations. Also, the radiometric processes that cause TB to decrease (scattering) during melt in the upper accumulation area need to be understood.

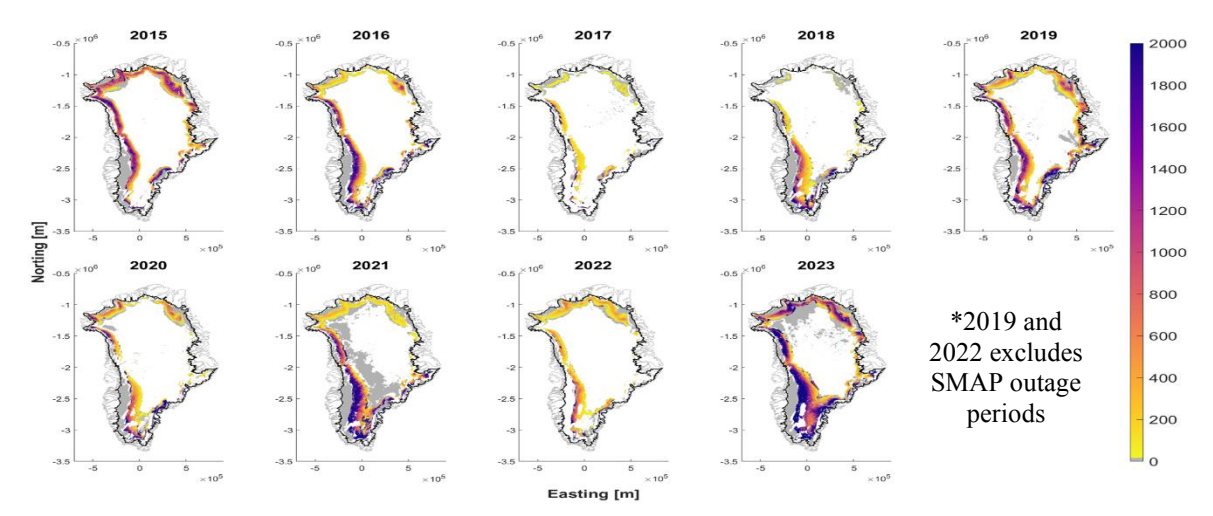


Fig. 3: SMAP retrieved total meltwater amounts (sum of evening MWA) per year for 2015-2023. Meltwater detected by decreased TB is masked and represented by grey color.

4. CONCLUSION

We quantified the total surface and subsurface meltwater amount over the Greenland ice sheet using the L-band observations from the SMAP mission. The retrieval algorithm was described, and validation results with in situ weather station measurements were provided. The results showed that the retrieval is in good agreement across the percolation zone but needs to be improved in the ablation and upper accumulation zones. A multifrequency algorithm is underway to determine the precise location and distribution of the meltwater. The results demonstrate the potential for advancing our understanding of ice sheet melt processes and dynamics. The approach will improve the projections of Greenland's contribution to global sea level rise in response to climate change and variability.

ACKNOWLEDGMENT

This work was carried out in part at the Jet Propulsion Laboratory, California Institute of Technology, under a contract with the National Aeronautics and Space Administration.

REFERENCES

- [1] M. R. Van Den Broeke *et al.*, "On the recent contribution of the Greenland ice sheet to sea level change," *Cryosphere*, vol. 10, no. 5, pp. 1933–1946.
- [2] B. Vandecrux et al., "Historical snow and ice temperature observations document the recent warming of the Greenland ice sheet," no. August, 2023.
- [3] A. J. Tedstone and H. Machguth, "Increasing surface runoff from Greenland's firn areas," *Nat. Clim. Chang.*, vol. 12, no. 7, pp. 672–676, 2022.
- [4] J. Harper *et al.*, "Greenland ice-sheet contribution to sea-level rise buffered by meltwater storage in firn," *Nature*, vol. 491, no. 7423, pp. 240–243, 2012.

- [5] R. Culberg, D. M. Schroeder, and W. Chu, "Extreme melt season ice layers reduce firn permeability across Greenland," *Nat. Commun.*, vol. 12, no. 1, pp. 1–9, 2021.
- [6] B. Vandecrux et al., "The firm meltwater Retention Model Intercomparison Project (RetMIP): Evaluation of nine firm models at four weather station sites on the Greenland ice sheet," Cryosphere, vol. 14, no. 11, pp. 3785–3810, 2020.
- [7] R. S. Fausto *et al.*, "Programme for Monitoring of the Greenland Ice Sheet (PROMICE) automatic weather station data," *Earth Syst. Sci. Data*, vol. 13, no. 8, pp. 3819–3845, 2021.
- [8] A. Colliander et al., "Ice Sheet Surface and Subsurface Melt Water Discrimination Using Multi-Frequency Microwave Radiometry," Geophys. Res. Lett., vol. 49, no. 4, 2022.
- [9] W. Abdalati and K. Steffen, "Snowmelt on the Greenland ice sheet as derived from passive microwave satellite data," *J. Clim.*, vol. 10, no. 2, pp. 165–175, 1997.
- [10] M. Tedesco, "Snowmelt detection over the Greenland ice sheet from SSM/I brightness temperature daily variations," *Geophys. Res. Lett.*, vol. 34, no. 2, pp. 1–6, 2007.
- [11] D. Houtz, et al., "Quantifying Surface Melt and Liquid Water on the Greenland Ice Sheet using L-band Radiometry," *Remote Sens. Environ.*, vol. 256, no. June 2020, 2021.
- [12] M. Mousavi et al., "Evaluation of Surface Melt on the Greenland Ice Sheet Using SMAP L-Band Microwave Radiometry," *IEEE J. Sel. Top. Appl. Earth Obs. Remote Sens.*, vol. 14, pp. 11439–11449, 2021.
- [13] D. G. Long, M. J. Brodzik, and M. Hardman, "Evaluating the effective resolution of enhanced resolution SMAP brightness temperature image products," *Front. Remote Sens.*, vol. 4, no. March, pp. 1–10, 2023.
- [14] S. Samimi, S. J. Marshall, B. Vandecrux, and M. MacFerrin, "Time-Domain Reflectometry Measurements and Modeling of Firn Meltwater Infiltration at DYE-2, Greenland," *J. Geophys. Res. Earth Surf.*, vol. 126, no. 10, Oct. 2021.